Human vs. Robotic Tactile Sensing: Detecting Lumps in Soft Tissue

James C. Gwilliam* jim.gwilliam@jhu.edu
Zachary Pezzementi† zap@cs.jhu.edu
Erica Jantho* ejantho1@jhu.edu
Allison M. Okamura‡ aokamura@jhu.edu
Steven Hsiao§ steven.hsiao@jhu.edu

Abstract

Humans can localize lumps in soft tissue using the distributed tactile feedback and processing afforded by the fingers and brain. This task becomes extremely difficult when the fingers are not in direct contact with the tissue, such as in laparoscopic or robot-assisted procedures. Tactile sensors have been proposed to characterize and detect lumps in robot-assisted palpation. In this work, we compare the performance of a capacitive tactile sensor with that of the human finger. We evaluate the response of the sensor as it pertains to robot-assisted palpation and compare the sensor performance to that of human subjects performing an equivalent task on the same set of artificial tissue models. Furthermore, we investigate the effects of various tissue parameters (lump size, lump depth, and surrounding tissue stiffness) on the performance of both the human finger and the tactile sensor. Using signal detection theory for determining tactile sensor lump detection thresholds, the tactile sensor outperforms the human finger in a palpation task.

Index Terms: H.5.2 [Information Interfaces and Presentation]: User Interfaces—Haptic I/O; H.1.2 [Models and Principles]: User/Machine Systems—Human Information Processing; I.5.2 [Pattern Recognition]: Design Methodology—Classifier Design and Evaluation

1 Introduction

During open surgery, surgeons rely on tactile sensations to guide manipulation and exploration [23], and assess the health of a wide variety of anatomical structures. Cancer, for example, is typically manifest as hard lumps (tumors) in the soft tissues of the breast, prostate, lungs, and other tissues [8]. Many studies have demonstrated that tumors are significantly stiffer than surrounding tissue, e.g. [16, 20, 32]. This facilitates the localization and assessment of tumors during open surgery, when the surgeon's fingertips are in direct contact with the tissue and tactile information is readily available. However, an increasing number of surgical resections are performed using minimally invasive surgery (MIS) or robot-assisted minimally invasive surgery (RMIS). These techniques provide numerous advantages over traditional open procedures, including increased dexterity, precision, and control, but eliminate the surgeon's natural tactile feedback. This makes palpation for lumps or tumors more difficult, especially because these structures are often beneath the tissue surface and cannot be detected visually.

Detection of lumps using tactile sensors presents unsolved problems in the acquisition, processing, and display of tactile data. The first challenge is the basic transduction of tactile data (tactile sensing). Touch can reveal shape, texture, friction, temperature, and other object properties. Researchers have implemented artificial tactile sensors for use with MIS endoscopic graspers, e.g. [7, 27, 35, 38], but no current tactile sensor is able to measure all the quantities perceived by the human finger. A second challenge is the subsequent computer processing of the transduced data to obtain useful information (tactile data processing). Approaches have included vision-based processing [6, 26], neural networks [5], and solid mechanics modeling [9, 10], but a rigorous comparison of methods is lacking. A final challenge is determining the most effective means for relaying the tactile information to a human user (tactile display). Researchers have displayed tactile information both visually [25, 29, 34, 41] and mechanically directly on the fingertips [15, 28, 29]. For the latter case, recreating the tactile sensations encountered during lump detection is hindered by the difficulty of designing appropriate electro-mechanical devices.

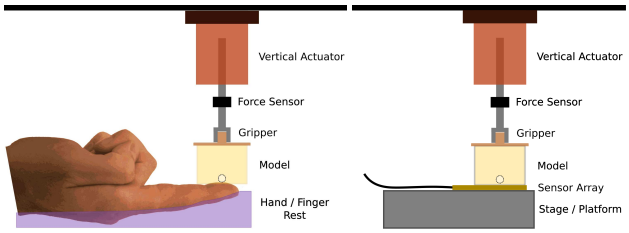

(a) Human psychophysics setup (b) Robot tactile sensor setup

Figure 1: Experimental setup conditions for both the psychophysics and tactile sensor experiments. (a) The right-hand index finger was fixed under a servo-controlled linear motor, which indented the rubber models to different depths into the finger based on the subject's response. (b) The tactile sensor is mounted on a rigid flat platform and the rubber models are indented stepwise into the tactile sensor.

Human sensing of lumps through palpation is a mechanically and neurophysiologically complex process. Due to the compliant nature of tissue, modeling the interaction between the fingers and the tissue requires a thorough understanding of contact mechanics and the nonlinear behavior of tissue. Some neurophysiology studies have investigated the relationship between a mechanical stimulus to the finger and human perception, but only rigid stimuli were represented [13, 18]. In palpation, the finger is in contact with compliant tissue, and both the tissue and finger change shape. Peine and Howe [30] evaluated the abilities of humans to detect hard lumps in soft tissue, with varying lump size and indentation velocity. They found that subjects sensed the deformation of the finger pad induced by the lump itself, and not the changes in finger pad pressure distribution.

The purpose of the current study is to compare the human finger with an artificial tactile sensor during a lump palpation task. Thus, it is important to note the spatio-temporal characteristics of each. The finger and tactile sensor are similar in that they both contain spatially arranged, touch-sensitive elements. However, they are distinguished by their spatio-temporal response, and the post-processing of the obtained information. The human finger contains a mixture of cutaneous sensing elements (mechanoreceptors), which differ in their receptive field size, location, sensitivity and adaptive properties, and spatial density within the finger. Cutaneous

*Department of Biomedical Engineering, Johns Hopkins University School of Medicine
†Department of Computer Science, Johns Hopkins University
‡Department of Mechanical Engineering, Johns Hopkins University
§Department of Neuroscience, Johns Hopkins University School of Medicine

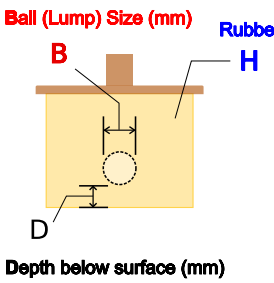

	00-10 (H10)			00-30 (H30)		
	B1	B2	B3	B1	B2	B3
(mm)	6.5	9.5	12.5	6.5	9.5	12.5
D1	1.5	1.5	1.5	1.5	1.5	1.5
D2	2.5	2.5	2.5	2.5	2.5	2.5
D3	3.5	3.5	3.5	3.5	3.5	3.5

Figure 2: Physical description of rubber models. Models differ in lump size (ball, B), embedded lump depth (depth, D), and hardness of surrounding rubber (hardness, H). All 18 models are represented in the table with dimensions in mm. The notation shown here is used throughout the paper.

mechanoreceptors are described as slowly adapting (SA) or rapidly adapting (RA), depending on their response to a step indentation. RA mechanoreceptors are also referred to as fast adapting (FA I) in other literature. Type I sensors (SA I and RA) have small receptive areas and well-defined boundaries, and are located close to the surface of the skin. Type II sensors (SA II and PC) have larger sensing areas, less clearly defined boundaries, and are embedded deeper within the skin [18]. The cutaneous sensing elements of the finger that contribute most in detecting lumps are the Merkel sensors (SA I), which are known to respond strongly to surface features (e.g. edges, corners, points, and curvature) and are responsible for form and texture perception. These mechanoreceptors are densely innervated in the skin (especially at the distal finger pad) with a density of about 70 sensors per cm^2, and have a spatial resolution of approximately 1 mm [19, 31].

In contrast, the tactile sensor used in this study has equally distributed and homogeneously organized sensing elements, identical in their temporal responses, placed at a density of 25 sensors per cm^2, with a spatial resolution no worse than the width of a single sensing element (2 mm) [33]. The temporal response of the finger's SA I mechanoreceptors and the tactile sensor elements are similar in that they both display a sustained output during constant static skin indentation.

While there have been studies focusing solely on human or artificial detection of lumps [4], few studies have directly compared human and tactile performance of lump detection in the same body of work [29, 37]. In this paper, we compare the performance of human and artificial tactile sensing during a palpation task. Unique from previous studies, we vary lump depth and surrounding material stiffness, in addition to lump size, and investigate how changing these physical parameters affects the performance of human and artificial tactile sensing. While human performance is quantified using standard psychophysics methods, performance of artificial tactile sensors is largely based on the methods, algorithms, and thresholds used in determining lump detection. The processing algorithms used in this study to determine tactile sensor performance are a variant of standard normalized cross-correlation applied both to model fitting and pattern matching, followed by thresholding. To the authors' knowledge this method is novel, but its effectiveness has not been rigorously compared to other methods in the literature. As such, we make our recorded tactile data publicly available as a source for benchmarking [1]. We encourage other groups to apply their tactile processing algorithms to this data and improve upon the results presented here.

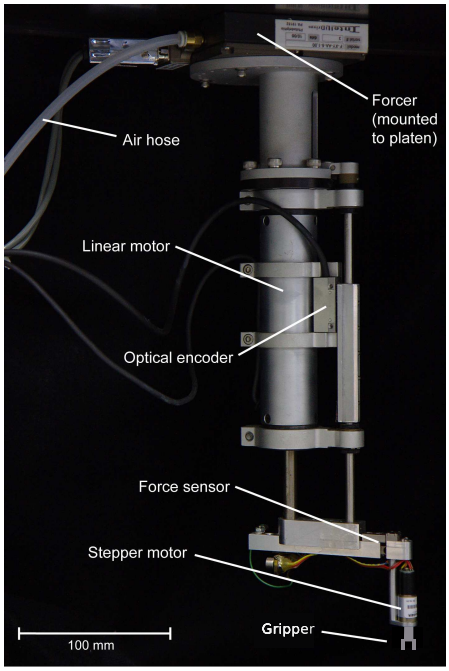

Figure 3: The platen-forcer stimulator system used in both human psychophysics and tactile sensor experiments. Figure adapted from [22].

2 Materials and Methods

2.1 Rubber Models

Rubber models were created to simulate hard lumps in soft tissue. Models were molded from Ecoflex 00-10 (softer) and 00-30 (harder) silicone rubber (Smooth-on Inc, Easton PA), where the suffix number represents the rubber hardness on the Shore 00 scale [3]. Models were shaped as cubic blocks measuring approximately 32 mm in each dimension. Lumps were machined from delrin as spheres with diameters of 6.5, 9.5, and 12.5 mm, and were embedded below the surface of the rubber at depths of 1.5, 2.5, and 3.5 mm. The combination of two rubber hardnesses (Shore 00-10, 00-30), three lump depths, and three lump sizes produce 18 distinct rubber models. A table of both model sets is shown in Figure 2. Two additional models without a lump served as baseline models, one for each rubber hardness. The models were imaged using ultrasound to verify that lumps were embedded at the proper depth from the surface. To limit of the number of variables in the experiment, we chose to make all lumps out of the same material (Delrin). Delrin is harder than most cancerous tissue, but provides a good contrast against the soft rubber for the purposes of this study. While tissue is difficult to model accurately due to its heterogeneity and variance according to location, we chose materials to represent tissue (ecoflex silicone rubber) and lumps (Delrin) which reasonably approximate an average equivalent contrast in stiffness to that found for lumps in breast [20] and prostate [17, 44] tissues.

2.2 Experimental Setup

Human psychophysics and tactile sensor experiments were both performed using a platen-forcer stimulation system (Figure 3). The stimulator consists of a servo-controlled linear motor (Baldor Electric Company Inc., Santa Clarita, CA) capable of providing controlled vertical displacements of the stimulus. The vertical position of the linear motor is measured using an optical encoder (Renishaw Inc., Hoffman Estates, IL), which provides position feedback and gives the system a 1 μm resolution over a travel stroke of 40 mm.

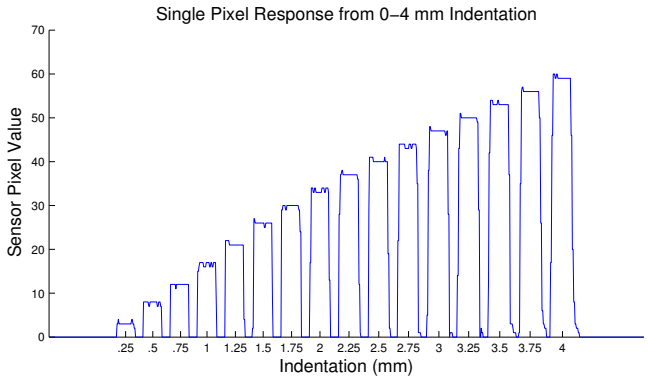

Figure 4: Single sensor pixel reading as a model was indented into the sensor stepwise from 0 to 4 mm in 0.25 mm increments. It is clear that the model broke contact with the sensor at each trial, before re-indenting to the new depth

The linear motor is attached to a forcer plate (platen), which glides across an overhead electromagnetic planar table (Intellidrives, Inc., Philadelphia, PA). The forcer contains two stepper motor modules, oriented at 90 degrees from each other, which control the horizontal (x and y) position of the stimulator to the target stimulation site with a resolution of 3 μm. A force sensor (Strain Measurement Devices Inc., Meriden, CT) and a small rotary stepper motor (Arsape Inc., Switzerland) are mounted to the bottom of the linear motor to detect applied forces and allow for rotation of the stimulus to the desired angle during stimulus presentation. A custom-made pneumatically controlled gripper attaches to and releases the different models between trials. A QNX realtime micro-kernel operating system (QNX Software Systems Inc., Ottawa, Canada) controls the pneumatic gripper, horizontal motion, and vertical displacement of the stimulator.

2.3 Robot Psychophysics Experiment

The tactile sensor used in this study was a custom DigiTacts system from Pressure Profile Systems [33], consisting of three smaller sensors, each of which is 12 mm $\times$ 8.5 mm and contains sensing elements with a spatial resolution of 1.8 mm, for a total of 72 sensor elements making up a 12 $\times$ 6 "tactile image" (Figure 5a). The total sensor system footprint is 12 mm $\times$ 25 mm, with 81% of the area being sensed, and the remaining 19% consisting of material between the individual sensing elements. The sensing modality was capacitive, with a sample rate of 30 Hz, sensitivity of 6.9×10^{-4} N/mm^2, and a sensing range of 0-0.14 N/mm^2, though our interaction forces never approached the upper range. The sensor was positioned on a flat rigid surface and fixed within the workspace of the stimulator (Figure 5b).

The stimulator was calibrated such that it would indent the models into the center of the sensor pad. Once the horizontal position was calibrated, each model was indented into the sensor from 0 to 4 mm in 250 μm increments. Once at the target indentation depth, the model was held in place for 250 ms, before breaking contact and then indenting to the next depth. Data used in this analysis are extracted from the static portion of the stimulus indentation (plateaus in Figure 4). For each trial (indentation), the data over the static 250 ms period were averaged for each sensor pixel, and compiled into a tactile image. Since we only considered data during the static period of contact between the model and sensor, effects of dynamic contact between the sensor and models, such as velocity of indentation, were not considered in this analysis.

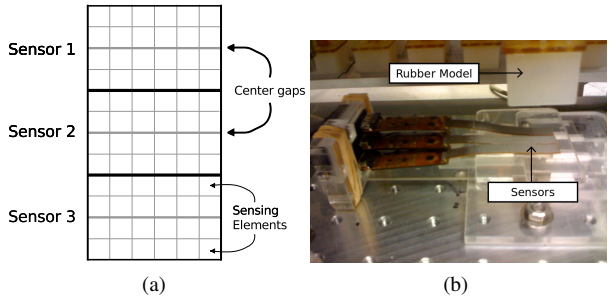

Figure 5: (a) Sensor layout. Three sensors are aligned adjacently, each containing a 6-by-4 array of 1.8 mm square sensing elements. 0.2 mm of (non-sensing) spacing is necessary between the individual sensors, except for the middle column of each sensor, where this gap is doubled. (b) The actual sensors mounted in the workspace of the robot stimulator.

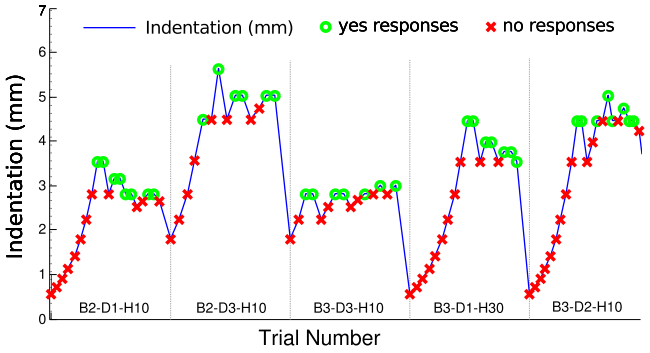

Figure 6: An example of the tracking algorithm for one subject. Positive responses (detection -o) are indicated in green, negative responses (non-detection -x) in red. Magnitude of stimulus intensity increments and decrements become smaller over the course of the tracking for a single model.

2.4 Human Psychophysics Experiment

The purpose of this task was to identify the minimum force and indentation depth required for the human finger to detect the lump for each rubber model. Each subject's right index finger was fixed (finger pad facing upward) in a finger holder using freshly molded dental gum (Kerr Corp., San Francisco, CA) which held the finger in place by the fingernail, while leaving the finger pad free for stimulation (Figure 1). Subjects were first trained with a set of 5 models, which spanned the largest and smallest lump size and lump depth. The platten forcer then selected each of the 18 models randomly to present to the finger. The initial stimulation depth was shallow (below threshold) and randomized (to prevent sensitization, conditioning, or decision bias). A model was indented to the target depth for a 500 ms period before breaking contact with the finger. Subjects controlled a mouse with the left hand to present their answers. A right click indicated negative detection, while a left click indicated positive detection. A subject's response initiated the next trial. The stimulator was programmed using a classical psychophysical tracking algorithm (staircase method) such that the indentation depth of the model into the finger changed as a function of the subjects' responses, using a "two-up, one-down" reversal paradigm, which provides a detection threshold of 71% [24]. The magnitude of the step size decreased with each reversal. A reversal was defined as changing the direction of the indentation step size from positive to negative, and back to positive, or vice versa.

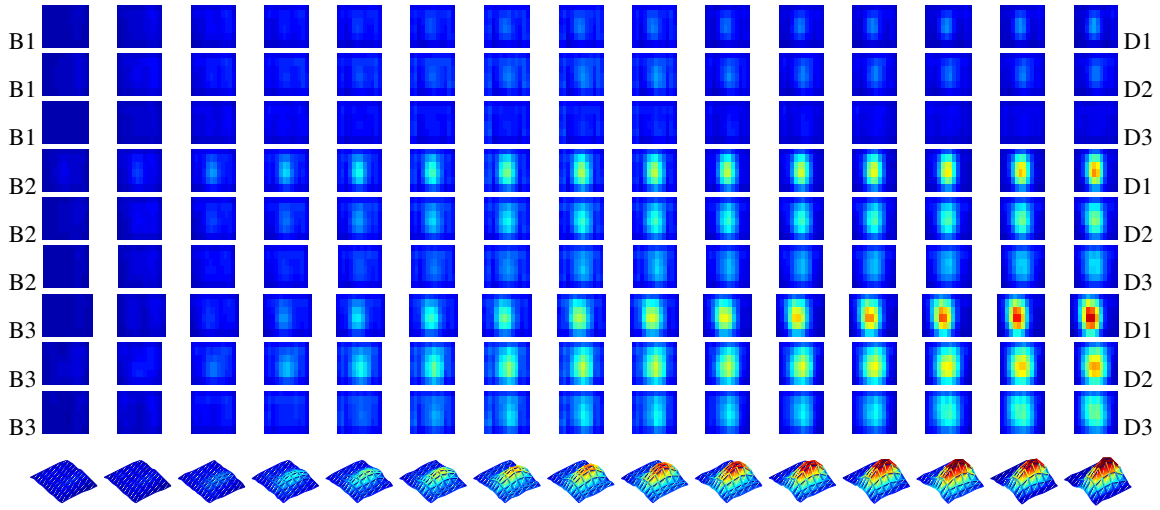

Figure 7: A qualitative pictoral assessment of sensor readings. Each square in the grid is a tactile image obtained from the tactile sensor. All 00-10 models are represented, with indentation depth increasing from left to right along the x-axis. Lump sizes (B, left) and embedded lump depths (D, right) are noted. The bottom row is a three-dimensional representation of the tactile sensor data obtained from the tactile sensor as model B2-D1-H10 was pressed into the sensor at 250 μm increments over a 4 mm range. A baseline image is subtracted from each tactile image to improve clarity.

The step size for stimulus indentation depth is given in (1), where X_N is the current indentation, X_0 is the initial indentation, and L_{dB} is the stimulus intensity in dB. N represents the most recent indentation.

$$X_N = X_0 * (10^{\frac{L_{dB}}{20}}) \tag{1}$$

Based on the subjects' response, L_{dB} was modified by 2 dB prior to the first reversal, 1 dB after the first and prior to the second reversal, and 0.5 dB thereafter, such that the step size magnitude decreased as the subject approached the threshold. Figure 6 shows the tracking algorithm for one subject across five randomly chosen models. Each section on the plot represents a single completed tracking algorithm for a rubber model.

The detection threshold for indentation depth ($X_{threshold}$) of each model was obtained using an arithmetic mean of the last five stimulus values of X_N so long as the range of the most recent 10 values (ΔX_{10}) were within a 2 dB range.

$$X_{threshold} = \frac{\sum_{i=1}^{5} X_{N+1-i}}{5} \iff \Delta X_{10} < 2dB \tag{2}$$

The force threshold was determined by averaging the five corresponding force values. This procedure was repeated for each of the 18 models. Data collected from subjects in this study was approved by the Johns Hopkins University Homewood Institutional Review Board. 10 students (7 female, 3 male) volunteered to participate in this study and were monetarily compensated for their participation.

3 Results

3.1 Tactile Sensor Results

Figure 7 shows qualitatively the sensor output as each of the 00-10 models are subjected to the 0 to 4 mm indentation protocol. Lump size and embedded lump depth are shown on the left and right side of the figure, respectively. Each image shown is obtained by subtracting a tactile baseline image (model with no lump) from the actual model data and smoothed with a two-dimensional Gaussian filter. Colormap values are scaled consistently across all images. The

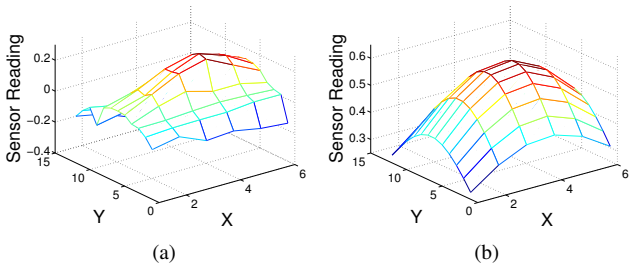

Figure 8: (a) Difference image between all models with a lump and all models without. (b) Our model, a Gaussian fit to this difference image.

clarity of the lump image obtained from the sensor fades with increasing depth between lump and tissue surface (D) and the size of the measured lump area increases with lump size (B), as expected.

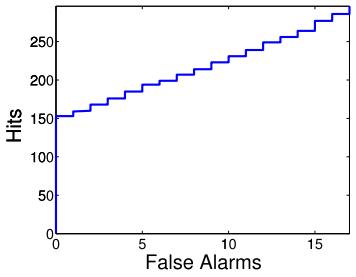

Figure 9: Receiver operating characteristic curve for detecting lumps using the artificial tactile sensors, while varying T.

Figure 7 (bottom row) shows a 3-dimensional representation of the data from a single model (B2-D1-H10) at each step of the tactile sensor 0 to 4 mm protocol. Each plot displays an increased indentation depth of the model into the sensor array. Indentation depth

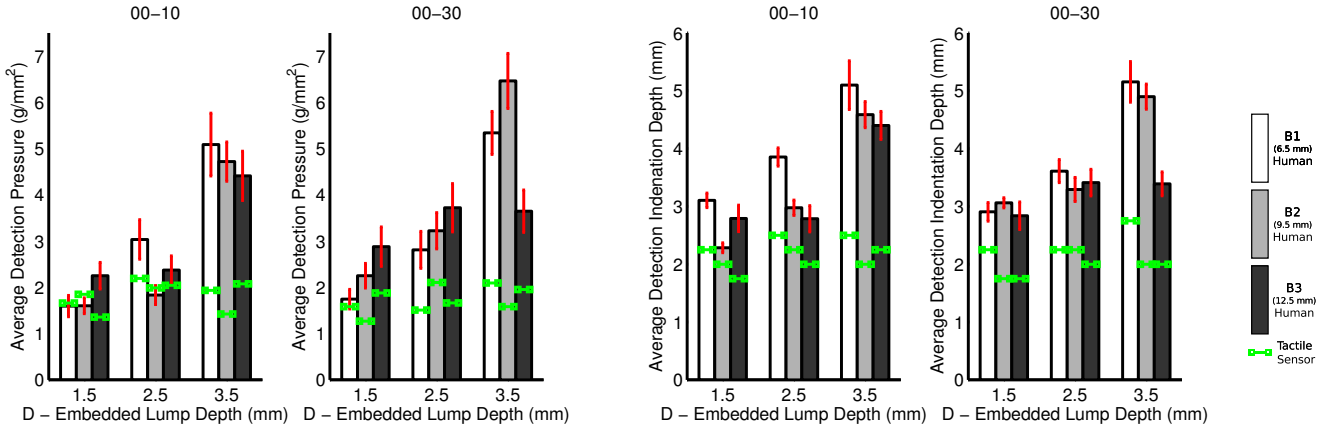

(a) Average Pressure for Lump Detection

(b) Average Indentation Depth for Lump Detection

Figure 10: Required detection pressure and indentation depth for human subjects and tactile sensor. Error bars reflect standard error. The left and right figure in each set correspond to the 00-10 and 00-30 materials, respectively. (a) Average pressure required for lump detection. (b) Average indentation depth required for lump detection. Tactile sensor detection pressures (a) and depths (b) are shown as green horizontal bars.

of the model into the sensor increases from left to right. The data shown are baseline normalized and Gaussian filtered.

We wished to determine at what indentation depth each lump could be reliably distinguished from the corresponding baseline model with no lump. We considered a machine learning-based approach, but determined that the small data set resulted in overfitting. We chose instead to use an approach rooted in signal detection theory. We explicitly modeled the shape of the response due to the lump in the tactile image. All tactile images were scaled so that each image, interpreted as a vector, would have norm 1, and an average image was computed for each class. The "no-lump" class average was then subtracted from the "lump" class average to get the difference image shown in Figure 8a. We then fit the parameters of a 2D Gaussian to this image by gradient descent to get our model of "lump presence", $\mathscr{L}$, shown in Figure 8b.

Consider the inner product between tactile images, $< I_a, I_b >$, to be a sum of pixel-wise multiplications between images I_a and I_b. We then computed the inner product between $\mathscr{L}$ and each tactile image in the data set, I_i, to estimate how strongly a lump is detected. The decision of whether to classify a given image as containing a lump or not consists simply of choosing a threshold, T, on this correlation value. Let D be the set of images decided to contain a lump. Then

$$L(I_i) =< I_i, \mathscr{L} > \quad (3)$$

$$D = \{i : L(I_i) > T\} \quad (4)$$

Finally, we must set a value for T. Figure 9 shows a receiver operating characteristic (ROC) curve, which displays all levels of performance attainable by varying T. To generate results most comparable to those of the human subjects, we chose to use the value which produces the most hits with no false positives, which corresponds to the lowest number of hits on the ROC curve. This choice resulted in the detections shown in green in Figure 10.

3.2 Human Psychophysics Results

Figure 10a shows the average pressure required for 10 human subject to detect the lumps. Although the stimulator force sensor recorded forces for both the human psychophysics and robot tactile sensor experiments, it was necessary for purposes of comparison to convert to a common unit of pressure since the contact areas between the sensor and the human finger pad differ. Finger pad widths were measured for each subject that participated in the psychophysics study, and the average value for all subjects was used to make an estimate of finger pad contact area on the model of

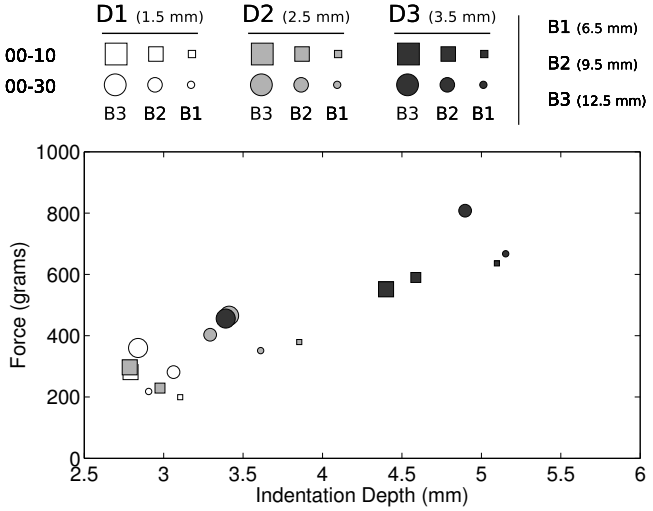

Figure 11: Cartesian representation of average detection forces and indentation depths required for lump detection for human subjects.

160 mm^2. Detection forces obtained in the psychophysics experiment were divided by this area to obtain the pressures shown. Similarly, detection pressures for the robot tactile sensor were obtained by dividing the detection forces by the area of the sensor array.

Figure 10b shows the average indentation depths required to detect the lumps. In general, the model must be indented further into the finger for lumps that are at deeper depths. Accordingly, the highest pressures are seen for the deepest embedded lumps. However, the role of lump size (curvature) is not as clearly discerned from this representation of the data. The smallest lump at the deepest depth (B1-D3) is the most difficult to detect. For both the detection pressures (Figure 10a) and indentation depths (Figure 10b), the tactile sensor outperforms the human finger in almost every case, requiring less pressure and indentation than the human finger to detect the same lump. This contrast in performance becomes more significant for deeper lumps.

Figure 11 shows the average forces and indentation depths required for human subjects to identify the lumps. This Cartesian display of the data shows what we might expect, that lumps closer to the surface cluster together at lower detection forces and indentation depths, while deeply embedded lumps are harder to identify.

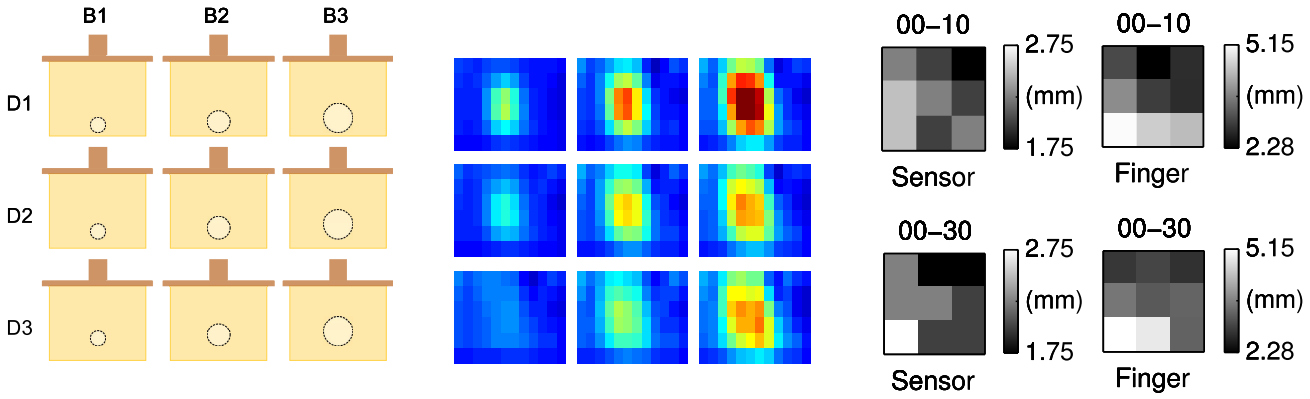

(a) Arrangement of data (b) Tactile images (c) Lump detection gradient images

Figure 12: Effects of lump size (curvature) and depth on detectability for both the human finger and robot tactile sensor. (a) Arrangement of data for all images in this figure. Lump depth displayed vertically and lump size displayed horizontally. (b) Tactile images at 3.25 mm indentation. (c) Lump detection gradient images display the indentation depths at which lumps were detected for both human finger and robot tactile sensor. Top and bottom row show 00-10 and 00-30 models respectively. The tactile sensor (left) and human finger (right) plots show different scales.

Figure 12b shows the tactile image produced at a 3.25 mm indentation depth across one set of rubber models. Comparing this array of images with Figure 12a at left, the effects of lump size (B) and embedded lump depth (D) on the resulting tactile images are can be visualized. Lump clarity fades or "blurs" as the lump depth increases and the size of the colored central region enlarges as lump size increases. The intensity of the pressure shown at the center of the tactile image corresponding to B3-D1 is largely affected by the resistance to displacement of the larger lump and the thin layer of rubber between the sensor and the lump (shallow embedded depth). Figure 12c presents the required indentation depths for lump detection spatially and chromatically for both the tactile sensor (left) and human finger (right). Each square or "pixel" corresponds with the models shown in Figure 12a. The color intensity of each pixel represents the indentation depth which was required to identify that lump. The sensor and finger plots use separate colormap scales, where the smallest (black) and largest (white) indentation depths represent easy and difficult lump identification, respectively. These images present a visual gradient describing how lump size and embedded depth affect perception. A comparison of Figures 12b and 12c illustrates the visual gradient of lump size and embedded depth on detectability. The lump detection gradients point in the same direction for both the sensor and finger plots.

4 Discussion

4.1 Human vs. Artificial Tactile Sensing

Figure 10 shows that the tactile sensor can detect lumps at lower indentation depths and pressures than the finger for this palpation task. This supports other findings that computerized or electronic palpation is more effective at detecting lumps than the human finger [36]. This finding also becomes significant in the context of minimally invasive and robot assisted minimally invasive surgery, where low forces and minimal manipulation of the tissue are desirable to prevent tissue and other internal structures from being punctured or damaged. Trejos et al. demonstrated that a tactile-sensing MIS instrument under robotic control reduces the maximum applied force to the tissue by more than 35% compared to manual palpation with the same instrument [42].

It should be noted that the method we used to detect lumps in the images from the artificial tactile sensor was not particularly optimized to improve the sensor's performance. A simple method was developed to demonstrate the capabilities of even a low-resolution sensor for this task. We have made our data available [1] for benchmarking tactile data processing methods for finding lumps in soft tissue. We invite other researchers to use this data to compare the performance of various algorithms against each other and the human performance data presented in this paper.

4.2 Effects of Lump Size and Depth

The three lump sizes used in this study likely did not span a large enough range to fully characterize the effects of lump size on detectability. Adams et al. used a larger number of spherical lumps (8) ranging from 1.6 to 12.7 mm in a lump detection task, and demonstrated that detectability of lumps increased with increasing lump size, though detectability saturated as the diameter of the lump approached the approximate width of the human finger pad [2]. In our study, lump sizes (ranging from 6.5 to 12.5 mm in diameter) approached the upper range of sizes used in [2]. It is likely that better contrast in results would have been obtained if slightly smaller lump sizes had been used in our study. Figure 12c shows that lumps that are closer to the surface and large are easiest to detect (black) while small lumps embedded deepest are most difficult to detect (white). Gradients for the sensor and finger are similar, and also correlate with the array of images shown in Figure 12b. Bloom et al. did a thorough analysis of the major stimulus parameters that affect detection of simulated breast lumps, including lump size, depth, hardness, and mobility, and similarly concluded that detectability of lumps increases as lumps are closer to the exposed surface of the tissue [4].

4.3 Softness Discrimination

Since most lumps or tumors are roughly spherical or ellipsoid in shape [40], detection of surface curvature is important for observing the presence of a lump and estimating its size. Goodwin et al. stimulated the human finger pad with rigid spherical stimuli of varying radii, and showed that slight changes in curvature (especially for stimuli smaller than a single finger pad) can drastically effect the firing rate of SA I mechanoreceptors [12, 14] and the perception [13] of the stimulus curvature. Similarly, Lamotte et al. showed that peak pressures vary inversely with the object radius, such that stronger responses would be evoked from the smaller lumps (larger curvature) [21]. Unlike the rigid objects used in these studies, our models can not be described as rigid, since a layer of soft rubber separates the spherical rigid lump from the finger pad. It is likely the rubber layer masks the effects of curvature (lump size) on detectability, especially for deeply placed lumps. In the strictest sense, detection of curvature for a hard lump embedded in a soft

elastic tissue becomes a question of softness discrimination. Lamotte et al. demonstrated that subjects discriminated the softness of objects with deformable surfaces equally under passive and active conditions [39], supporting the sufficiency of the passive stimulus approach used in the human portion of this study. Because of the curvature of the lump, there is less elastic material separating the surface of the tissue from the center of the hard lump than at the edges of the lump, making the lump feel harder at the center. This claim makes sense when viewed with Figures 12a and 12b, where peak pressures occur at the "hardest" locations, or in other words, at the center where the smallest amount of soft tissue separates the hard lump from the finger or tactile sensor. This property is exaggerated for larger lumps (e.g. B3-D1 in Figure 12b), since they are more resistant to displacement in the surrounding tissue. Therefore, equivalent indentations for models with different lump sizes, but similar embedded depths, would result in larger measured pressures for the larger lump.

4.4 Factors Affecting Human Performance

Current evidence suggests that when subjects are given equal access to the sensory input from the afferent fibers, there is no difference in perception in active or passive tactile tasks [43], indicating that an active or passive approach in this task (with all other conditions held constant) would likely have yielded equivalent results. However, it should be noted that the passive, one-dimensional (orthogonal motion only) method of stimulus presentation used in this experiment is distinctly different from the active palpation techniques taught in medical schools. In normal palpation for lumps, surgeons combine motions orthogonal to the surface of the tissue with scanning motions parallel to the surface. Such exploratory motions are thought to be more effective at driving the mechanoreceptors of the fingers and enhance the percepts of form [11, 14], texture [39], and location of tumors in tissue. Movement is thought to improve performance by enhancing the firing rates of the afferent fibers and provide information about the proprioceptive movements of the finger. In this experiment, the finger is held static while the model is indented into the finger. We hypothesize that a factor limiting the performance of the finger was that it remained motionless during the presentation of stimuli. Conducting the experiment passively in this way allows us to accurately control the indentation velocity, depth, and location of the stimuli, as well as enable measurement of forces. However, it is possible that the absence of lateral scanning movement may have prevented the subjects from performing optimally. Since the robotic tactile sensor was passive by nature, it seemed appropriate to conduct the human portion of the experiment in a passive manner in order to compare performance of the human to the tactile sensor.

A second factor that may have affected human performance is the nature of the psychophysical approach used in this study. During each trial (indentation), subjects answered whether they detected the ball or not at a particular indentation depth. In addition, every model used in the human portion of the study contained an embedded lump. Human performance might have been different if a true 2AFC (two alternative forced choice) protocol was used, in which subjects would compare models with and without embedded lumps.

A final factor that may have improved sensor performance relative to the human finger is the fact that the entire sensor area was used in the signal detection theory analysis. An interesting comparison for future work would be comparison to the sensor results obtained using only an area of the sensor equivalent to the average area of a single human fingerpad.

5 Conclusions and Future Work

In this study, we show that a standard tactile sensor and data processing methods can detect hard lumps in soft tissue with lower indentation depths and pressures than the human finger in a passive palpation task. Lumps closer to the surface are easier to detect, since less rubber tissue separates the finger from the lump. Larger lumps are easier to detect, likely because their larger size produces a greater force per unit of indentation in resistance to movement through the tissue when palpated. Tactile sensor data is made publicly available for benchmarking purposes. Currently, we are investigating the neurophysiological response of the mechanoreceptors in monkeys to determine the neural coding of detecting lumps in soft tissue. Physiological results will be compared with the results of this study.

Acknowledgements

This work was supported by National Science Foundation grant 0722943, NIH grants NS34086 and NS18787, a National Science Foundation Graduate Fellowship, and a Link Foundation Fellowship. The authors thank Zhicheng Lai for help with programming the stimulator, Bill Nash and Bill Quinlan for making the rubber models, and Frank Dammann and Justin Killebrew for assistance with data analysis.

References

[1] https://infrastructure.lcsr.jhu.edu/Tactile_sensors, Oct 2009.

[2] C. K. Adams, D. C. Hall, H. S. Pennypacker, M. K. Goldstein, L. L. Hench, M. C. Madden, G. H. Stein, and A. C. Catania. Lump detection in simulated human breasts. *Perception and Psychophysics*, 20(3):163–167, 1976.

[3] ASTM. Standard test method for rubber property: Durometer hardness. http://dx.doi.org/10.1520/D2240-05.

[4] H. S. Bloom, E. L. Criswell, H. S. Pennypacker, A. C. Catania, and C. K. Adams. Major stimulus dimensions determining detection of simulated breast lesions. *Perception and Psychophysics*, 32(3):251–260, 1982.

[5] S. Charlton, P. Sikka, and H. Zhang. Extracting contact parameters from tactile data using artificial neural networks. In *Proc. IEEE Int'l Conference on Systems, Man and Cybernetics*, pages 3954–3959, 1995.

[6] N. Chen, R. Rink, and H. Zhang. Efficient edge detection from tactile data. In *Proc. IEEE Int'l Conference on Intelligent Robots and Systems*, pages 386–391, 1995.

[7] J. Dargahi and S. Najarian. An integrated force-position tactile sensor for improving diagnostic and therapeutic endoscopic surgery. *Biomedical Materials Engineering*, 14(2):151–166, 2004.

[8] P. Dario. Tactile sensing: Technology and applications. *Sensors and Actuators*, 1(1):251–256, 1991.

[9] V. Egorov, S. Ayrapetyan, and A. P. Sarvazyan. Prostate mechanical imaging: 3-d image composition and feature calculations. *IEEE Transactions on Medical Imaging*, 25(10):1329–1340, 2006.

[10] V. Egorov and A. P. Sarvazyan. Mechanical imaging of the breast. *IEEE Transactions on Medical Imaging*, 27(9):1275–1287, 2008.

[11] A. Goodwin, K. John, and A. Marceglia. Tactile discrimination of curvature by humans using only cutaneous information from the fingerpads. *Experimental Brain Research*, 86(3):663–672, 1991.

[12] A. W. Goodwin, A. S. Browning, and H. E. Wheat. Representation of curved surfaces in responses of mechanoreceptive afferent fibers innervating the monkey's fingerpad. *Journal of Neuroscience*, 15:798–810, 1995.

[13] A. W. Goodwin, K. T. John, and A. H. Marceglia. Tactile discrimination of curvature by humans using only cutaneous information from the fingerpads. *Experimental Brain Research*, 86(3):663–672, 1991.

[14] A. W. Goodwin, V. G. Macefield, and J. W. Bisley. Encoding of object curvature by tactile afferents from human fingers. *Journal of Neurophysiology*, 78(6):2881–2888, 1997.

[15] R. Howe, W. Peine, D. Kantarinis, and J. Son. Remote palpation technology. *IEEE Engineering in Medicine and Biology Magazine*, 14(3):318–323, 1995.

[16] K. Hoyt, B. Castaneda, M. Zhang, P. Nigwekar, P. A. Di'Sant'agnese, J. V. Joseph, J. Strang, D. J. Rubens, and K. J. Parker. Tissue elasticity properties as biomarkers for prostate cancer. *Cancer Biomarkers*, 4(4-5):213–225, 2008.

[17] V. Jalkanen, B. M. Andersson, A. Bergh, B. Ljungberg, and O. A. Lindahl. Prostate tissue stiffness as measured with a resonance sensor system: a study on silicone and human prostate tissue in vitro. *Medical and Biology Engineering and Computing*, 44(7):593–603, 2006.

[18] R. Johansson and A. Vallbo. Tactile sensory coding in the glabrous skin of the human hand. *Trends in Neuroscience*, 6(1):27–32, 1983.

[19] K. Johnson and J. Phillips. Tactile spatial resolution. i. two-point discrimination, gap detection, grating resolution, and letter recognition. *Journal of Neurophysiology*, 46(6):1177–1192, 1981.

[20] T. A. Krouskop, T. M. Wheeler, F. Kallel, B. S. Garra, and T. Hall. Elastic moduli of breast and prostate tissues under compression. *Ultrasonic Imaging*, 20(4):260–274, 1998.

[21] R. H. LaMotte and M. A. Srinivasan. Responses of cutaneous mechanoreceptors to the shape of objects applied to the primate fingerpad. *Acta Psychologica (Amst)*, 84(1):41–51, 1993.

[22] J. W. Lane, P. J. Fitzgerald, J. M. Yau, I. Pembeci, and S. S. Hsiao. A tactile stimulator for studying passive shape perception. *Journal of Neuroscience Methods*, 2009 (In Press).

[23] S. Lederman and R. Klatzky. Sensing and displaying spatially distributed fingertip forces in haptic interfaces for teleoperator and virtual environment systems. *Presence: Teleoperators and Virtual Environments*, 8(1):86–103, 1999.

[24] H. Levitt. Transformed up-down methods in psychoacoustics. *The Journal of the Acoustical Society of America*, 49(2B):467–477, 1971.

[25] A. P. Miller, W. J. Peine, J. S. Son, and Z. T. Hammoud. Tactile imaging system for localizing lung nodules during video assisted thoracoscopic surgery. In *Proc. IEEE Int'l Conference on Robotics and Automation*, pages 2996–3001, 2007.

[26] C. Muthukrishnan, D. Smith, D. Myers, J. Rebman, and A. Koivo. Edge detection in tactile images. In *Proc. IEEE Int'l Conference on Robotics and Automation*, pages 1500–1505, 1987.

[27] M. Ottermo, O. Stavdahl, and T. Johansen. Palpation instrument for augmented minimally invasive surgery. In *Proc. IEEE Int'l Conference on Intelligent Robots and Systems*, pages 3960–3964, 2004.

[28] M. Ottermo, O. Stavdahl, and T. Johansen. A remote palpation instrument for laparoscopic surgery: Design and performance. *Minimally Invasive Therapy and Allied Technologies*, 18:1–14, 2009.

[29] M. V. Ottermo, M. M. Ovstedal, T. Lango, O. Stavdahl, Y. Yavuz, T. A. Johansen, and R. Marvik. The role of tactile feedback in laparoscopic surgery. *Surgical Laparoscopy Endoscopy and Percutaneous Techniques*, 16(6):390–400, 2006.

[30] W. Peine and R. Howe. Do humans sense finger deformation or distributed pressure to detect lumps in soft tissue? In *Proc. ASME Dynamic Systems and Control Division*, pages 273–278, 1998.

[31] J. Phillips and K. Johnson. Tactile spatial resolution. ii. neural representation of bars, edges, and gratings in monkey primary afferents. *Journal of Neurophysiology*, 46(6):1192–1203, 1981.

[32] S. Phipps, T. H. J. Yang, F. K. Habib, R. L. Reuben, and S. A. McNeill. Measurement of tissue mechanical characteristics to distinguish between benign and malignant prostatic disease. *Urology*, 66(2):447–450, 2005.

[33] PPS. DigiTacts II^{TM}, tactile array sensor evaluation kit with digital output. Pressure Profile Systems. Available from: <http://www.pressureprofile.com/UserFiles/File/DigiTactsII Evaluation/Specification Sheet.pdf>.

[34] M. Ramezanifard, S. Sokhanvar, J. Dargahi, W.-F. Xie, and M. Packirisamy. Graphical reproduction of tactile information of embedded lumps for mis applications. In *Proc. IEEE Symposium on Haptic Interfaces for Virtual Environments and Teleoperator Systems*, pages 247–252, 2008.

[35] N. Rao, J. Dargahi, M. Kahrizi, and S. Prasad. Design and fabrication of a microtactile sensor. In *Proc. IEEE Canadian Conference on Electrical and Computer Engineering*, pages 1167–1170, 2003.

[36] A. Sarvazyan. Computerized palpation is more sensitive than human finger. In *Proc. 12th Int'l Symposium on Biomedical Measurements and Instrumentation*, pages 523–524, 1998.

[37] A. Sarvazyan. Mechanical imaging:: A new technology for medical diagnostics. *International Journal of Medical Informatics*, 49(2):195–216, 1998.

[38] S. Schostek, C.-N. Ho, D. Kalanovic, and M. O. Schurr. Artificial tactile sensing in minimally invasive surgery - a new technical approach. *Minimally Invasive Therapy and Allied Technologies*, 15(5):296–304, 2006.

[39] M. Srinivasan and R. LaMotte. Tactual discrimination of softness. *Journal of Neurophysiology*, 73:88–101, 1995.

[40] D. L. Stippel, H. G. Brochhagen, M. Arenja, J. Hunkemller, A. H. Hlscher, and K. T. E. Beckurts. Variability of size and shape of necrosis induced by radiofrequency ablation in human livers: a volumetric evaluation. *Annals of Surgical Oncology*, 11(4):420–425, 2004.

[41] A. Trejos, J. Jayender, M. Perri, M. Naish, R. Patel, and R. Malthaner. Experimental evaluation of robot-assisted tactile sensing for minimally invasive surgery. In *Proc IEEE Int'l Conference on Biomedical Robotics and Biomechatronics*, pages 971–976, 2008.

[42] A. L. Trejos, J. Jayender, M. P. Perri, M. D. Naish, R. V. Patel, and R. A. Malthaner. Robot-assisted tactile sensing for minimally invasive tumor localization. *The International Journal of Robotics Research*, 28:1188–1133, 2009.

[43] F. Vega-Bermudez, K. O. Johnson, and S. S. Hsiao. Human tactile pattern recognition: active versus passive touch, velocity effects, and patterns of confusion. *Journal of Neurophysiology*, 65(3):531–546, 1991.

[44] M. Zhang, P. Nigwekar, B. Castaneda, K. Hoyt, J. V. Joseph, A. di Sant'Agnese, E. M. Messing, J. G. Strang, D. J. Rubens, and K. J. Parker. Quantitative characterization of viscoelastic properties of human prostate correlated with histology. *Ultrasound in Medicine and Biology*, 34(7):1033–1042, 2008.